Int J Adv Manuf Technol (2006) 28: 82–91
DOI 10.1007/s00170-004-2352-8

ORIGINAL ARTICLE

Jingzhou Yang · Karim Abdel-Malek

Verification of NC machining processes using swept volumes

Received: 27 May 2004 / Accepted: 27 July 2004 / Published online: 29 June 2005

Abstract A numerically controlled (NC) machining verification method is developed based on a formulation for delineating the volume generated by the motion of a cutting tool on the workpiece (stock). The motion of a cutting tool is modeled as a surface undergoing a sweep operation along another geometric entity where machine tool trajectory includes translational and rotational movements. A rank-deficiency condition is imposed on the Jacobian of the sweep to determine the singular surfaces. Singular entities are then intersected to determine sub-entities that may exist on the boundary of the volume. A perturbation method is used to identify the boundary envelope of the material volume to be removed. Numerical examples

illustrating the formulation are presented. Benefits of this method are its ability to depict and visualize the manifold and to compute a value for the volume.

Keywords Boundary envelope · Jacobian · Manifold · NC machining process · Volume

1 Introduction

Integrated computer-aided design (CAD), computer-aided manufacturing (CAM), and computer numerical control (CNC) manufacturing systems are widely used in today's manufacturing industries to increase productivity and efficiency. Complicated part geometry and the additional machining axes in five-axis NC machining compared to three-axis tool paths generated by the current CAM systems may generate some errors, such as cutter gouging and tool interference. Traditionally, prototypes are used to verify the tool paths before the actual machining, but that is time-consuming and expensive.

J. Yang (✉) · K. Abdel-Malek
Virtual Soldier Research Program, Center for Computer-Aided Design,
Department of Mechanical & Industrial Engineering,
The University of Iowa,
111 Engineering Research Facility, Iowa City, IA 52242, USA
E-mail: jyang@engineering.uiowa.edu
Tel.: +1-319-3532249,
Fax: +1-319-3840542

Numerically controlled (NC) verification refers to computer modeling and simulation used in the validation of NC machining programs before they are executed on a computer-controlled machine. Currently, most commercial NC simulation systems use sampling points to represent the cutter geometry and a G-buffer to represent the machined part surfaces. When the cutter moves along the tool paths, the distance between the cutter and the part surface is calculated and updated. However, calculating the distances between the hundreds of sampling points of the cutter and the part surface is computationally expensive. While recent advances in this field have been made in terms of speed and accuracy, formulations for verifying machining processes with more than three axes have been very limited. Early work on this subject is due to Wang and Wang [1], and important works addressing the representation of the boundary of the removed material have increased in recent years. For example, Boussac and Crosnier [2] suggest a representation of swept volumes generated by the motion of deformable objects based on the topological properties of n-dimensional manifolds.

Methods of dual quad tree structures and boundary representation were applied to modeling the parts cut by a wire for electric discharge machining (EDM) verification [3]. The sweep-envelope approach is used to address the NC verification issues [4–6]. The sweep-envelope differential equation method is probably the most elegant method to date that has proven to be suitable for NC verification [7, 8]. Some of the works that have addressed NC verification but have not used swept volume methods include Voelker and Hunt [9], Menon and Voelcker [10], Oliver and Goodman [11], Narvekar et al. [12], Takata et al. [13], Jerard and Drysdale [14, 15], Koren and Lin [16], Menon and Robinson [17], Oliver [18], Liang et al. [19], Liu et al. [20], Lee [21], Lo [22], Chiou et al. [23, 24], Elber and Cohen [25], Balasubramaniam et al. [26, 27], Rao and Sarma [28], Jensen et al. [29], Bohez [30], Mann and Bedi [31], Yoon et al. [32], Bedi et al. [33], Gray et al. [34, 35], Fussell et al. [36], Lauwers et al. [37], Jun et al. [38], Bohez et al. [39], and Langeron et al. [40].

The report by Abdel-Malek and Yeh [41] presented the first introduction of the Jacobian rank-deficiency method as an ap-

plication for treating consecutive sweep operations of up to four parameters. Abdel-Malek et al. [42] expanded this method, presenting a complete rigorous mathematical formulation adapted from kinematics to study the acceleration function on singular surfaces.

This paper presents the extension of that work into a broadly applicable formulation using swept volume theory and perturbation method. This is a closed formulation of sweeps with n-parameters. Furthermore, adapting this work to numerically controlled verification proves that the formulation is suitable for a variety of fields where sweeping is the underlying action.

There have been many works that have treated the topic of swept volumes (refer to the references surveyed by Abdel-Malek and Yeh [43] and by Blackmore et al. [44]). Other recent works that have demonstrated analytic methods for computing swept volumes are Ahn et al. [45], Elber [46], Ling and Chase [47], and Sourin and Pasko [48].

We shall first present a formulation for characterizing the topological space produced as a result of the sweep of a geometric entity (representing the cutting tool) in space along its cutting path, and due to multiple axes motion. The goal is to identify the boundary to this manifold with singularities. The resulting boundary of the space that is nearly a manifold with singularities will be identified and its volume computed. A perturbation algorithm will be applied to determine the boundary of the manifold. It will be shown that this formulation allows for an exact computation of the volume, and thus the accuracy of the verification process is very high.

2 Formulation

2.1 Determination of singular surfaces

The motion of a cutting tool in an NC milling or EDM process can be characterized as the sweep of a surface (enveloping the tool) along some path. Consider a geometric entity that envelops the cutting tool and is parametrized in terms of one or more variables as a (3×1) vector given by $\boldsymbol{k}(\boldsymbol{u})$, where $\boldsymbol{u} = [u_1 \dots u_n]^T$, and where the tool can be represented as a curve, a surface, or an entity in n-dimensional space. In order to generalize the formulation, we shall also consider boundaries imposed on $\boldsymbol{k}(\boldsymbol{u})$ in the form of constraints on the parameters u_i characterized by inequality constraints in the form of $u_i^L \le u_i \le u_i^U$. Because of the multi-axis operation of NC machines, the tool surface will be swept several times, each along or about an axis. This path will be considered as a second geometric entity parametrized in terms of one or more variables as a (3×1) vector $\boldsymbol{\Psi}_1(v_1)$. This entity also has a boundary defined by $v_1^L \le v_1 \le v_1^U$. The manifold generated by the sweep of $\boldsymbol{k}(u_1, \dots, u_n)$ on $\boldsymbol{\Psi}_1(v_1)$ is defined by the vector

$$\boldsymbol{N}_1(\boldsymbol{q}) = [x(\boldsymbol{q})\ y(\boldsymbol{q})\ z(\boldsymbol{q})]^T = \boldsymbol{R}_1(v_1)\boldsymbol{k}(\boldsymbol{u}) + \boldsymbol{\Psi}_1(v_1)\ , \tag{1}$$

where $\boldsymbol{N}_1(\boldsymbol{q}) = [x\ y\ z]^T$, $\boldsymbol{q}$ is the vector of generalized coordinates defined by $\boldsymbol{q} = [q_1 \ \dots \ q_n]^T = [u_1 \ \dots \ u_n\ v_1]^T$, and $\boldsymbol{R}_1(v_1)$ is the (3×3) rotation matrix defining the orientation of the cutting tool. In fact, $\xi(\boldsymbol{q})$ characterizes the set of all points that belong to the manifold. Another axis motion yields an expanded swept volume in the form of

$$\boldsymbol{N}_2(\boldsymbol{q}) = \boldsymbol{R}_2(v_2)\boldsymbol{N}_1(\boldsymbol{q}) + \boldsymbol{\Psi}_2(v_2) = \boldsymbol{R}_2\boldsymbol{R}_1\boldsymbol{k} + \boldsymbol{R}_2\boldsymbol{\Psi}_1 + \boldsymbol{\Psi}_2\ , \tag{2}$$

where now $\boldsymbol{q} = [u_1 \ \dots \ u_n\ v_1\ v_2]^T$. Another axis motion yields a modified set defined by

$$\boldsymbol{N}_3 = \boldsymbol{R}_3\boldsymbol{R}_2\boldsymbol{R}_1\boldsymbol{k} + \boldsymbol{R}_3\boldsymbol{R}_2\boldsymbol{\Psi}_1 + \boldsymbol{R}_3\boldsymbol{\Psi}_2 + \boldsymbol{\Psi}_3\ . \tag{3}$$

The generalized case yields a space characterized by the vector function $\boldsymbol{\xi} = [\xi^{(x)}\ \xi^{(y)}\xi^{(z)}]^T$, such that

$$\boldsymbol{\xi}(\boldsymbol{q}) = \prod_{i=1}^{m} \boldsymbol{R}_i\boldsymbol{k} + \sum_{j=1}^{m-1}\left(\prod_{i=j+1}^{m} [\boldsymbol{R}_i]\,\boldsymbol{\Psi}_j\right) + \boldsymbol{\Psi}_m\ , \tag{4}$$

where $\boldsymbol{q} = [\boldsymbol{u}^T\ \boldsymbol{v}^T]^T$, $\boldsymbol{u} = [u_1 \ \dots \ u_n]^T$, and $\boldsymbol{v} = [v_1 \ \dots \ v_m]^T$. The aim is to identify this space and its boundary, and to compute its volume, which is the removed material.

To impose inequality constraints, it was shown that a constraint of the form $q_i^{\min} \le q_i \le q_i^{\max}$ can be transformed into an equation by introducing a new set of generalized coordinates λ_i such that

$$q_i = a_i + b_i \sin\lambda_i\ i = 1, \dots, n+m\ , \tag{5}$$

where $a_i = (q_i^{\max} + q_i^{\min})/2$ and $b_i = (q_i^{\max} - q_i^{\min})/2$ are the mid-point and half-range, respectively. Equation 5 can be written as $\boldsymbol{q} = \boldsymbol{\Pi}(\boldsymbol{\lambda})$. At any point in the manifold, a vector constraint equation $\boldsymbol{H}(\boldsymbol{q}^*)$ with the parametrized inequality constraints can be defined as

$$\boldsymbol{H}(\boldsymbol{q}^*) = \begin{bmatrix} \boldsymbol{\xi}^{(x)}(\boldsymbol{q}) - x \\ \boldsymbol{\xi}^{(y)}(\boldsymbol{q}) - y \\ \boldsymbol{\xi}^{(z)}(\boldsymbol{q}) - z \\ q_i - 0.5(q_i^{\max} + q_i^{\min}) - 0.5(q_i^{\max} - q_i^{\min})\sin\boldsymbol{\lambda}_i \end{bmatrix} = \boldsymbol{0},$$
$$i = 1, \dots, n+m\ , \tag{6}$$

where $\boldsymbol{q}^* = [\boldsymbol{u}^T\ \boldsymbol{v}^T\ \boldsymbol{\lambda}^T]^T$ is the vector of all generalized coordinates and $\boldsymbol{\lambda} = [\lambda_1 \ \dots \ \lambda_{n+m}]^T$. Note that although $(n+m)$ new variables (l_i's) have been added, $(n+m)$ equations have also been added to the constraint vector function without affecting the dimensionality of the problem.

In order to have a well-posed formulation, constraints that are used to model the geometry of this problem should be independent, except at certain critical surfaces in the manifold (implicit function theorem) when the Jacobian becomes singular. It is important, therefore, that there be no open sets in the space of the generalized parameters in which the constraints are redundant. Redundancy occurs when the Jacobian $\boldsymbol{H}_{\boldsymbol{q}^*} = \partial\boldsymbol{H}/\partial\boldsymbol{q}^*$, is rank-deficient, and which will subsequently define varieties (singularity surfaces) in the manifold.

The Jacobian is expanded as

$$\boldsymbol{H}_{\boldsymbol{q}^*} = \begin{bmatrix} \xi_{q_1}^{(x)} & \xi_{q_2}^{(x)} & \dots & \xi_{q_{n+m}}^{(x)} & 0 & 0 & 0 & 0 \\ \xi_{q_1}^{(y)} & \xi_{q_2}^{(y)} & \dots & \xi_{q_{n+m}}^{(y)} & 0 & 0 & 0 & 0 \\ \xi_{q_1}^{(z)} & \xi_{q_2}^{(z)} & \dots & \xi_{q_{n+m}}^{(z)} & 0 & 0 & 0 & 0 \\ 1 & 0 & 0 & 0 & -b_1 \cos\lambda_1 & 0 & \dots & 0 \\ 0 & 1 & 0 & 0 & 0 & -b_2 \cos\lambda_2 & \dots & 0 \\ \dots & \dots & \dots & \dots & \dots & \dots & \dots & \dots \\ 0 & 0 & 0 & 1 & 0 & 0 & \dots & -b_{n+m} \cos\lambda_{n+m} \end{bmatrix} = \begin{bmatrix} \boldsymbol{\xi_q} & \boldsymbol{0} \\ \boldsymbol{I} & \boldsymbol{q_\lambda} \end{bmatrix}, \tag{7}$$

where the notation $x_{q_1}^{(x)}$ denotes the partial derivative of $x^{(x)}$ with respect to q_1, $\boldsymbol{\xi_q} = \partial\boldsymbol{\xi}/\partial\boldsymbol{q}$ is the upper left corner sub-matrix (only with respect to $\boldsymbol{q}$), $\boldsymbol{q_\lambda} = \partial\boldsymbol{q}/\partial\boldsymbol{\lambda}$ is the diagonal lower right corner matrix, and $\boldsymbol{I}$ is the identity matrix.

For an $(n+m)$-parameter verification, the Jacobian $\boldsymbol{H}_{\boldsymbol{q}^*}(\boldsymbol{q}^*)$ row-rank-deficiency yields the following three types of singular behavior.

2.1.1 Type I singularity sets

When matrix $\boldsymbol{\xi_q}$ has rank-deficiency, the singularity sets are type I. In order to make the matrix $\boldsymbol{\xi_q}$ rank-deficient of order (d), it is necessary to determine all square sub-Jacobians, which are analytic functions. Equating the determinants to zero yields a number of analytic equations to be solved simultaneously. The zeros of the resulting equations are sets of constant, generalized coordinates, and type I singularity sets are characterized by the following:

$$S^{(1)} \equiv \left\{ \boldsymbol{p} \in \boldsymbol{q} : \text{Rank}[\boldsymbol{\xi_q}(\boldsymbol{u}, \boldsymbol{p})] < 3, \text{ for some constant subset of } \boldsymbol{q} \right\}, \tag{8}$$

where $\boldsymbol{q} = \{\boldsymbol{u}^T \ \boldsymbol{p}^T\}^T$, $\boldsymbol{u} \cap \boldsymbol{p} = \emptyset$.

2.1.2 Type II singularity sets:

If the matrix $\boldsymbol{q_\lambda}$ is row-rank-deficient (i.e., $b_i \cos\lambda_i$ is zero for some $i = 1, \dots, (n+m)$), then q_i has reached a limit, and the corresponding $x_{\boldsymbol{q}}$ is studied for row-rank-deficiency. When certain parameters reach their limits, e.g., $\partial\boldsymbol{q}^{\text{limit}} = [q_i^{\text{limit}}, q_j^{\text{limit}}, q_k^{\text{limit}}]^T$, the corresponding diagonal elements in the matrix $\boldsymbol{q_\lambda}$ will be equal to zero. Therefore, the corresponding matrix is subjected to the rank-deficiency criterion, where $\boldsymbol{H}_{\boldsymbol{q}^*}$ will take on the following form:

$$\boldsymbol{H}_{\boldsymbol{q}^*} \sim \begin{bmatrix} \boldsymbol{\xi}_{q_1} \dots \boldsymbol{\xi}_{q_i} \boldsymbol{\xi}_{q_j} \boldsymbol{\xi}_{q_k} \dots \boldsymbol{\xi}_{q_{n+m}} \\ 0 \dots 1 \ 0 \ 0 \dots \ 0 \\ 0 \dots 0 \ 1 \ 0 \dots \ 0 \\ 0 \dots 0 \ 0 \ 1 \dots \ 0 \end{bmatrix} \tag{9}$$

and where the three columns pertaining to $\boldsymbol{\xi}_{q_i}$, $\boldsymbol{\xi}_{q_j}$, and $\boldsymbol{\xi}_{q_k}$ are removed such that the rank-deficiency criteria are applied again.

The type II singularity set is defined as:

$$S^{(2)} \equiv \left\{ \boldsymbol{p} = [\hat{\boldsymbol{p}} \cup \partial\boldsymbol{q}^{\text{limit}}] : \text{Rank}\,[\boldsymbol{\xi_q}(\boldsymbol{w}, \partial\boldsymbol{q}^{\text{limit}})] < 3, \text{ for some } \hat{\boldsymbol{p}} \in \boldsymbol{q}, \ \dim(\partial\boldsymbol{q}^{\text{limit}}) \le (n-3) \right\}, \tag{10}$$

where $\boldsymbol{q} = \{\boldsymbol{w}^T \ \partial\boldsymbol{q}^{\text{limit}}\}^T$, $\boldsymbol{w} \cap \partial\boldsymbol{q}^{\text{limit}} = \emptyset$, $\boldsymbol{w} = \{\boldsymbol{u}^T \ \hat{\boldsymbol{p}}^T\}^T$.

2.1.3 Type III singularity sets

Type III sets are all sets that are composed of the combination of joints at their limits and are defined by:

$$S^{(3)} \equiv \left\{ \boldsymbol{p} \in \boldsymbol{R}^{(n+m-2)}, \boldsymbol{p} \equiv \partial\boldsymbol{q}^{\text{limit}} = [q_i^{\text{limit}}, q_j^{\text{limit}}, \dots] \right\}; \text{ where } i \neq j. \tag{11}$$

2.2 Perturbation method

The singular set is a combination of the above three types of singularity sets: $S^{(1)}$, $S^{(2)}$, and $S^{(3)}$, such that

$$S = S^{(1)} \cup S^{(2)} \cup S^{(3)} = \left\{ \boldsymbol{p}^1, \boldsymbol{p}^2, \dots, \boldsymbol{p}^{ns} \right\}, \tag{12}$$

where ns is the total number of singular vectors $\boldsymbol{p}$. Substituting these singular vectors into the manifold generated by $n+m$-parameter machining in Eq. 4 yields ns parametric singular entities:

$$\boldsymbol{\chi}^i(\boldsymbol{u}^i | \boldsymbol{p}^i), \text{ for } i = 1, \dots, ns. \tag{13}$$

In general, unless otherwise stated, those entities are parametric surfaces and are denoted by singular surfaces. The vector $\boldsymbol{u}^i$ represents the joint coordinates used as the parameters of the singular surface i, and $\boldsymbol{p}^i$ is the constant singular vector.

Intersections between these singular surfaces may exist. The intersection curves, also called singular curves, partition a singular surface into a number of sub-regions called sub-surfaces, denoted by $\boldsymbol{\psi}^i$. Singular curves are considered as higher-order singularities. It is necessary to determine these curves, such that every sub-surface can be defined, as shown in Fig. 1.

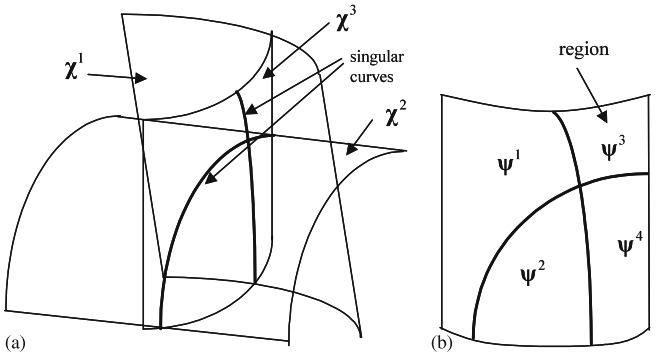

Fig. 1. The intersection and partition of singular surfaces

To compute the intersection curves between two parametric singular surfaces defined by:

$$\boldsymbol{\chi}^1(u, v),\ u_1 \le u \le u_2,\ v_1 \le v \le v_2 \tag{14a}$$

$$\boldsymbol{\chi}^2(s, w),\ s_1 \le s \le s_2,\ w_1 \le w \le w_2\,. \tag{14b}$$

The method proposed by Abdel-Malek and Yeh [49] is employed. Substitute the following equations

$$\boldsymbol{\chi}^1(\boldsymbol{u}^1) - \boldsymbol{\chi}^2(\boldsymbol{u}^2) = \mathbf{0} \tag{15}$$

and joint limitations of $\boldsymbol{u}^1$ and $\boldsymbol{u}^2$ into the augmented constraint function $\boldsymbol{H}$. The intersection curve can then be traced following the procedure described by Abdel-Malek and Yeh [49].

Upon determining the intersections between all singular surfaces, each sub-surface can be identified. Sub-surfaces may exist inside the manifold or its outer boundaries. It is important to distinguish these two types of sub-surfaces, because the interior sub-surfaces may represent some barriers to the motion of cutter tools, while the outer sub-surfaces are boundaries of the manifold. To determine whether sub-surface $\boldsymbol{\psi}^i$ is internal or on the boundary, a perturbation of a selected point on the sub-surface is carried out. The idea is that the points, perturbed along the normal direction, on both sides of the sub-surface, should satisfy the equation of constraints, Eq. 6, if the sub-surface is inside the manifold, rather than on the boundary. Any point on the sub-surface can be selected, provided that it is not on an intersection curve.

For a sub-surface $\psi^i(\boldsymbol{u}^i) = \psi^i(u, v)$, the variables u, v are the parameters. At any point on the sub-surface, suppose the corresponding joint coordinate vector is z^0, which can be partitioned as:

$$z^0 = \left[u^0\ v^0\ \boldsymbol{p}^{i^T}\right]^T\,. \tag{16}$$

The normal vector of a singular surface can be calculated as:

$$\boldsymbol{n}^0 = \left(\frac{\partial \boldsymbol{\psi}^i}{\partial u} \times \frac{\partial \boldsymbol{\psi}^i}{\partial v}\right) \Big/ \left\| \frac{\partial \boldsymbol{\psi}^i}{\partial u} \times \frac{\partial \boldsymbol{\psi}^i}{\partial v} \right\|\,. \tag{17}$$

For a small perturbation $\partial\varepsilon$ about this point and along the normal vector $\boldsymbol{n}^0$, the coordinates of the perturbed point can be calculated as:

$$\boldsymbol{\xi}^p = \boldsymbol{\psi}^i(u^0, v^0) \pm \partial\varepsilon \boldsymbol{n}^0\,. \tag{18}$$

For the perturbed point to exist within the manifold, an admissible time vector should exist that satisfies Eq. 6, such that a solution to the following equations exists:

$$\begin{bmatrix} \boldsymbol{\xi}^p - \boldsymbol{\Phi}(\boldsymbol{q}) \\ \boldsymbol{q} - \boldsymbol{\Pi}(\boldsymbol{\lambda}) \end{bmatrix} = 0\,. \tag{19}$$

The modified Newton–Raphson method with the generalized inverse method is used to determine whether this nonlinear system of equations has a solution. The sub-surface $\boldsymbol{\psi}^i$ is an internal surface if and only if solutions to Eq. 19 exist for both perturbations of $\pm\partial\varepsilon$. Otherwise, the surface will be on the boundary of the manifold.

2.3 Calculation of the volume

Because this formulation yields closed-form surface equations for describing the boundary of the manifold, it is now possible to apply the divergence theorem to compute the material volume removed that is essential to the NC verification. The contribution of a variety $\boldsymbol{\chi}^{(i)}(\boldsymbol{u})$, where $\boldsymbol{u} = [q_1\ q_2]^T$, to the volume of a manifold with unit normal $\hat{\boldsymbol{n}}^{(i)}$ using the divergence theorem is given by:

$$3V = \iint_A \boldsymbol{\chi}^{(i)}(\boldsymbol{u}) \hat{\boldsymbol{n}}^{(i)}\, \mathrm{d}A\,. \tag{20}$$

The area is given by $\mathrm{d}A = \|\boldsymbol{\chi}^{(i)}_{q_1} \times \boldsymbol{\chi}^{(i)}_{q_2}\|\, \mathrm{d}q_1\, \mathrm{d}q_2$ and for a variety that is a parametric entity, the normal vector is written as $\hat{\boldsymbol{n}}^{(i)} = \frac{\boldsymbol{\chi}^{(i)}_{q_1} \times \boldsymbol{\chi}^{(i)}_{q_2}}{\|\boldsymbol{\chi}^{(i)}_{q_1} \times \boldsymbol{\chi}^{(i)}_{q_2}\|}$. Substituting for $\mathrm{d}A$ and for $\hat{\boldsymbol{n}}^{(i)}$ into Eq. 20, the volume V of a solid model enclosed by varieties is the summation of the contribution of all boundary varieties as (note that $\boldsymbol{n}$ is not a unit vector):

$$V = \frac{1}{3} \sum_i^{\eta} \iint_A \boldsymbol{\chi}^{(i)}(q_1, q_2) \boldsymbol{n}^{(i)}\, \mathrm{d}q_1\, \mathrm{d}q_2\,. \tag{21}$$

3 An introductory example

Consider the NC verification of a process involving the motion of a cutting tool represented by the parametric vector $\boldsymbol{\Gamma}(\boldsymbol{u}) = [10\cos u\ 10\sin u\ 10]^T$. The first motion will be a rotational motion of $\boldsymbol{\Gamma}$ and the second motion will be translational along an axis. The rotation matrix is

$$\boldsymbol{R}_2(v_2) = \begin{bmatrix} \cos v_2 & 0 & -\sin v_2 \\ \sin v_2 & 0 & \cos v_2 \\ 0 & -1 & 0 \end{bmatrix}\,.$$

The translational path is $\boldsymbol{\Psi}_2(v_2) = [20\cos v_2\ 20\sin v_2\ 0]^T$ followed by another machining axis with

$$\boldsymbol{R}_1(v_1) = \begin{bmatrix} \cos v_1 & \sin v_1 & 0 \\ \sin v_1 & -\cos v_1 & 0 \\ 0 & 0 & 1 \end{bmatrix}\,,$$

and $\boldsymbol{\Psi}_1(v_1) = [0\ 0\ 50]^T$ is subject to the following constraints $0 \le u \le 2\pi$, $-\pi/4 \le v_1 \le 5\pi/4$, $-\pi/4 \le v_2 \le \pi/2$, as shown in Fig. 2. The manifold is characterized by three parameters:

$$\boldsymbol{\xi}(\boldsymbol{q}) = \begin{bmatrix} 10\cos q_1 \cos q_2 \cos q_3 - 10\sin q_1 \sin q_3 \\ -10\cos q_1 \sin q_2 + 20\cos q_1 \cos q_2 \\ 10\sin q_1 \cos q_2 \cos q_3 + 10\cos q_1 \sin q_3 \\ -10\sin q_1 \sin q_2 + 20\sin q_1 \cos q_2 \\ 10\sin q_2 \cos q_3 \\ +10\cos q_2 + 20\sin q_2 + 50 \end{bmatrix}\,, \tag{22}$$

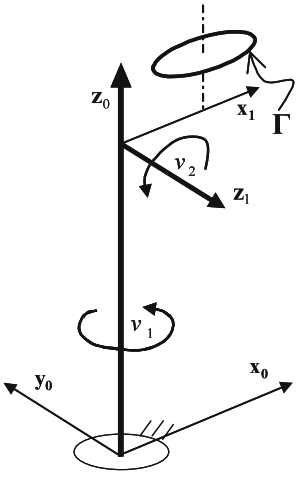

Fig. 2. A three-parameter verification

where $\boldsymbol{q} = [v_1\ v_2\ u]^T = [q_1\ q_2\ q_3]^T$. The Jacobian matrix is derived as:

$$\boldsymbol{H}_{q^*} = \begin{bmatrix} \boldsymbol{\xi_q}\ \boldsymbol{0} \\ \boldsymbol{I}\ \boldsymbol{q_\lambda} \end{bmatrix}, \tag{23}$$

where

$$\boldsymbol{\xi_q} = \begin{bmatrix} -10(c_2(2+c_3)s_1 - s_1s_2 + c_1s_3) & -10(c_1(c_2+(2+c_3)s_2)) & -10(c_3s_1 + c_1c_2s_3) \\ 10(c_1(c_2(2+c_3) - s_2)) & -10s_1(c_2+(2+c_3)s_2) & 10(c_1c_3 - c_2s_1s_3) \\ 0 & 10(c_2(2+c_3) - s_2) & -10s_2s_3\ , \end{bmatrix}$$

$c_i = \cos q_i,\ s_i = \sin q_i\ ,$

$$\boldsymbol{q_\lambda} = \begin{bmatrix} -\frac{3\pi}{4}\cos\lambda_1 & 0 & 0 \\ 0 & -\frac{3\pi}{4}\cos\lambda_2 & 0 \\ 0 & 0 & -\pi\cos\lambda_3 \end{bmatrix}, \boldsymbol{\lambda} = [\lambda_1\ \lambda_2\ \lambda_3]^T.$$

Type I Jacobian singularities

Since $[\boldsymbol{\xi_q}]$ is a (3×3) block matrix,

the determinant of this (3×3) matrix can be computed and simplified as:

$$\mathrm{Det}[\boldsymbol{\xi_q}] = -2000(\cos q_2(2+\cos q_3) - \sin q_2)\sin q_3 = 0\ . \tag{24}$$

Solving Eq. 24 yields $q_3 = 0$ or $q_3 = \pi$. Therefore, Jacobian singular sets are $\boldsymbol{p}^1 = \{q_3 = 0\}$, $\boldsymbol{p}^2 = \{q_3 = \pi\}$.

Type II singularities

For each parameter to reach its limit, there are only two variables left that will define a parametric surface. Therefore, there is no type II singularity set.

Type III singularities

Type III singular sets include $\boldsymbol{p}^3 = \{q_1 = -\pi/4\}$, $\boldsymbol{p}^4 = \{q_1 = 5\pi/4\}$, $\boldsymbol{p}^5 = \{q_2 = -\pi/4\}$, and $\boldsymbol{p}^6 = \{q_2 = \pi/2\}$.

Substituting those singularity sets into Eq. 22 yields six singular surfaces, denoted by $\boldsymbol{\chi}_1$ to $\boldsymbol{\chi}_6$ as shown in Fig. 3. There are intersections between these six singular surfaces; the intersection curves will divide the singular surface into several subsurfaces.

For example, surface $\boldsymbol{\chi}_3$ is parameterized by two variables, q_2 and q_3. The intersection curves between surface $\boldsymbol{\chi}_3$ and other singular surfaces can be traced by the method proposed by Abdel-Malek and Yeh [49]. All of the curves can be plotted in the surface parametric space (q_2,q_3) shown in Fig. 4. The two curves of $\boldsymbol{c}^1$ and $\boldsymbol{c}^2$ are the intersections with surface $\boldsymbol{\chi}_4$. The surface $\boldsymbol{\chi}_3$ also intersects with surfaces $\boldsymbol{\chi}_6$ and $\boldsymbol{\chi}_1$ in curves $\boldsymbol{c}^3$ and $\boldsymbol{c}^4$, respectively. To determine whether each sub-surface is a boundary or internal sub-surface of the workspace, the perturbation method of Eq. 18 is applied. For example, consider the point p^1 on the sub-surface $\boldsymbol{\psi}^1$, which has the following set of joint coordinates:

$$z^0 = [q_1\ q_2\ q_3]^T = [-\pi/4\ 0.4\ 3.4]^T\ .$$

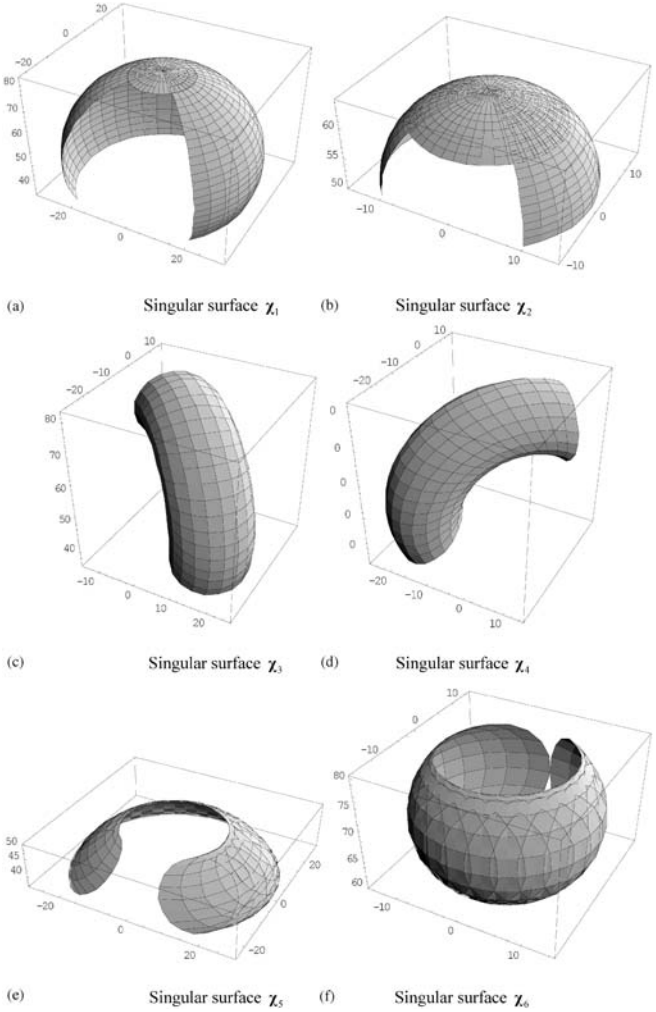

Fig. 3. Singular surfaces

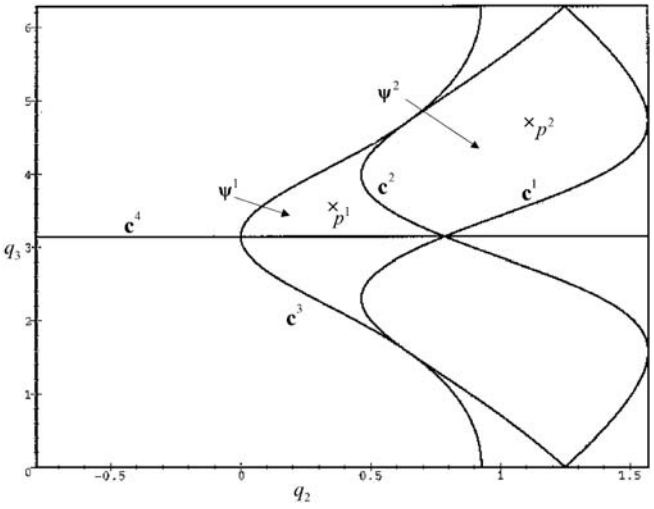

Fig. 4. Singular surface is divided into several sub-surfaces

The normal vector at the point p^1 to $\boldsymbol{\psi}^1$ can be calculated by:

$$\boldsymbol{n}^0 = \left(\frac{\partial \boldsymbol{\psi}^1}{\partial q_2} \times \frac{\partial \boldsymbol{\psi}^1}{\partial q_3}\right) \Big/ \left\| \frac{\partial \boldsymbol{\psi}^1}{\partial q_2} \times \frac{\partial \boldsymbol{\psi}^1}{\partial q_3} \right\| = [0.098\ -0.452\ 0.887]^T \ .$$

For a small perturbation $\partial\varepsilon = +0.1$, the coordinates of the perturbed point are computed as:

$$\boldsymbol{\xi}^{p^+} = \boldsymbol{\psi}^1(\boldsymbol{z}^0) + 0.1\boldsymbol{n}^0 = [6.513\ -1.812\ 63.418]^T \ .$$

Solving Eq. 19 by the modified Newton–Raphson method, the iterations converge to a solution $\boldsymbol{z} = [2.321\ 1.222\ -3.502]^T$. Similarly, the other perturbed point $\boldsymbol{x}^{p^-}$ due to $\partial\varepsilon = -0.1$ can be computed as:

$$\boldsymbol{\xi}^{p^-} = \boldsymbol{\psi}^1(\boldsymbol{z}^0) - 0.1\boldsymbol{n}^0 = [6.494\ -1.721\ 63.241]^T \ .$$

The iterations also converge to a solution $\boldsymbol{z} = [2.393\ 1.231\ -3.463]^T$. Thus, both perturbation points are inside the workspace. Therefore, the sub-surface $\boldsymbol{\psi}^1$ is an internal sub-surface. For example, select the point p^2 on the sub-surface $\boldsymbol{\psi}^2$, which has joint coordinates $\boldsymbol{z}^0 = [q_1\ q_2\ q_3]^T = [-\pi/4\ 1.0\ 4.4]^T$. The normal vector at this point is calculated as:

$$\boldsymbol{n}^0 = [0.671\ 0.653\ 0.351]^T \ .$$

For a small positive perturbation $\partial\varepsilon = +0.1$, the perturbed point is

$$\boldsymbol{\xi}^{p^+} = [-6.211\ -7.245\ 69.646]^T \ .$$

Solving the corresponding equation of Eq. 19, a convergence solution is obtained as $\boldsymbol{z} = [2.276\ 1.114\ 1.882]^T$. However, a solution cannot be found for the negative perturbation point with $\partial\varepsilon = -0.1$. This indicates that $\boldsymbol{\psi}^2$ is a boundary sub-surface of the workspace.

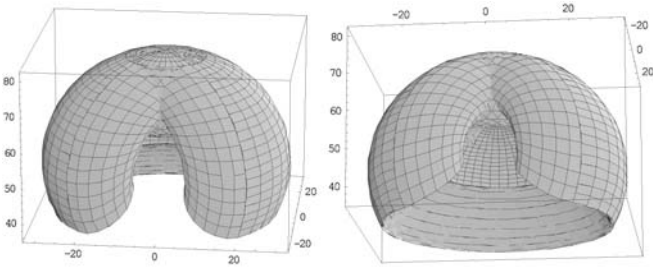

Fig. 5. Two views of removed volume

Using this technique, the boundary sub-surfaces of each singular surface are identified. These surfaces are depicted in Fig. 5, from two different points of view. The volume enclosed by these surfaces is the workspace.

4 Four-parameter NC verification and volume

Consider the machining of a conical part shown in Fig. 6. The accessible output set (swept volume) and its boundary of the material to be removed has to be computed. The tool used has a hemispherical tip (Fig. 7). The tool surface is given by the equation of a sphere as:

$$\Gamma(q_3, q_4) = \begin{bmatrix} 2\cos q_3 \cos q_4 \\ 2\cos q_3 \sin q_4 \\ 2\sin q_3 \end{bmatrix} , \tag{25}$$

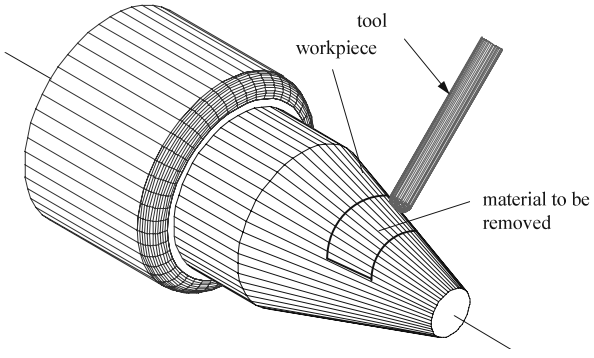

Fig. 6. Machining operation with four parameters

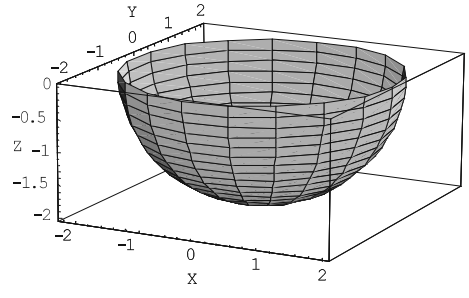

Fig. 7. Cutter's surface

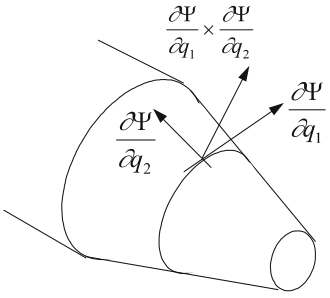

Fig. 8. Defining normal and tangent vectors

and constrained as $(-\pi/2) \le q_3 \le 0$ and $0 \le q_4 \le 2\pi$. The workpiece is a conical section given by:

$$\Psi(q_1, q_2) = \begin{bmatrix} q_2 \tan(\pi/6) \cos q_1 \\ q_2 \tan(\pi/6) \sin q_1 \\ q_2 \end{bmatrix} . \tag{26}$$

The material to be removed is constrained to $0 \le q_1 \le \pi$ and $15^{"} \le q_2 \le 25^{"}$.

Two tangent unit vectors to the surface can be obtained by $\frac{\partial\Psi}{\partial q_1} = [-\sin q_1 \cos q_1\ 0]^T$ and $\frac{\partial\Psi}{\partial q_2} = [\frac{c\cos q_1}{\sqrt{c^2+1}}\ \frac{c\sin q_1}{\sqrt{c^2+1}}\ \frac{1}{\sqrt{c^2+1}}]^T$, where $c = \tan(\pi/6)$. A third orthonormal vector can be obtained by computing the cross product of the two unit vectors as shown in Fig. 8. The rotation matrix can then be written as:

$$\boldsymbol{R}(q_1) = \begin{bmatrix} -\sin q_1 & \frac{c\cos q_1}{\sqrt{c^2+1}} & \frac{c\cos q_1}{\sqrt{c^2+c^4}} \\ \cos q_1 & \frac{c\sin q_1}{\sqrt{c^2+1}} & \frac{c\sin q_1}{\sqrt{c^2+c^4}} \\ 0 & \frac{1}{\sqrt{c^2+1}} & \frac{-c^2}{\sqrt{c^2+c^4}} \end{bmatrix} . \tag{27}$$

The accessible set can be written as:

$$\boldsymbol{\xi}(\boldsymbol{q}) = \begin{bmatrix} 0.577 q_2 \cos q_1 - 2\cos q_3 \cos q_4 \sin q_1 \\ +1.732 \cos q_1 \sin q_3 + \cos q_1 \cos q_3 \sin q_4 \\ \\ 2\cos q_1 \cos q_3 \cos q_4 + 0.577 q_2 \sin q_1 \\ +1.732 \sin q_1 \sin q_3 + \cos q_3 \sin q_1 \sin q_4 \\ \\ q_2 - \sin q_3 + 1.732 \cos q_3 \sin q_4 \end{bmatrix} , \tag{28}$$

subject to the inequality constraints defined above.

Table 1. Volume calculation

Variety	Parametric limits	Volume contribution
$\zeta^{(1)}$	$15 \le q_2 \le 25,\ -\pi/2 \le q_3 \le 0$	72.552
$\zeta^{(2)}$	$15 \le q_2 \le 25,\ -\pi/2 \le q_3 \le 0$	72.552
$\zeta^{(3)}$	$0 \le q_1 \le \pi,\ -\pi/2 \le q_3 \le 0$	626.142
$\zeta^{(4)}$	$0 \le q_1 \le \pi,\ -\pi/2 \le q_3 \le 0$	2879.08
$\zeta^{(5)}$	$0 \le q_1 \le \pi,\ 15 \le q_2 \le 25$	0
$\zeta^{(6)}$	$0 \le q_1 \le \pi,\ 15 \le q_2 \le 25$	0
$\zeta^{(7)}$	$0 \le q_1 \le \pi,\ 15 \le q_2 \le 25$	712.094
$\zeta^{(8)}$	$-\pi/2 \le q_3 \le 0,\ \pi/2 \le q_4 \le 3\pi/2$	25.1327
$\zeta^{(9)}$	$-\pi/2 \le q_3 \le 0,\ \pi/2 \le q_4 \le 3\pi/2$	25.1327
$\zeta^{(10)}$	$15 \le q_2 \le 25,\ 0 \le q_4 \le 2\pi$	0
$\zeta^{(11)}$	$-\pi/2 \le q_3 \le 0,\ \pi/2 \le q_4 \le 3\pi/2$	25.1327
$\zeta^{(11)}$	$-\pi/2 \le q_3 \le 0,\ \pi/2 \le q_4 \le 3\pi/2$	25.1327
$\zeta^{(12)}$	$15 \le q_2 \le 25,\ 0 \le q_4 \le 2\pi$	0
	Total	4462.9508

Applying the same procedures as the introduction example, 28 singularity sets are obtained as:

$\boldsymbol{p}^1 = \{q_1 = 0, q_3 = -\pi/2\}$, $\boldsymbol{p}^2 = \{q_1 = 0, q_4 = 0\}$,
$\boldsymbol{p}^3 = \{q_1 = 0, q_4 = \pi\}$, $\boldsymbol{p}^4 = \{q_1 = \pi, q_3 = -\pi/2\}$,
$\boldsymbol{p}^5 = \{q_1 = \pi, q_4 = 0\}$, $\boldsymbol{p}^6 = \{q_1 = \pi, q_4 = \pi\}$,
$\boldsymbol{p}^7 = \{q_2 = 15, q_3 = -\pi/2\}$, $\boldsymbol{p}^8 = \{q_2 = 15, q_4 = \pi/2\}$,
$\boldsymbol{p}^9 = \{q_2 = 15, q_4 = -\pi/2\}$, $\boldsymbol{p}^{10} = \{q_2 = 25, q_3 = -\pi/2\}$,
$\boldsymbol{p}^{11} = \{q_2 = 25, q_4 = \pi/2\}$, $\boldsymbol{p}^{12} = \{q_2 = 25, q_4 = -\pi/2\}$,
$\boldsymbol{p}^{13} = \{q_3 = 0, q_4 = 0\}$, $\boldsymbol{p}^{14} = \{q_3 = 0, q_4 = \pi/2\}$,
$\boldsymbol{p}^{15} = \{q_3 = 0, q_4 = \pi\}$, $\boldsymbol{p}^{16} = \{q_3 = 0, q_4 = 3\pi/2\}$,
$\boldsymbol{p}^{17} = \{q_3 = 0, q_4 = 2\pi\}$, $\boldsymbol{p}^{18} = \{q_3 = -\pi/2, q_4 = 0\}$,
$\boldsymbol{p}^{19} = \{q_1 = 0, q_2 = 15\}$, $\boldsymbol{p}^{20} = \{q_1 = 0, q_2 = 25\}$,
$\boldsymbol{p}^{21} = \{q_1 = 0, q_3 = 0\}$, $\boldsymbol{p}^{22} = \{q_2 = 15, q_3 = 0\}$,
$\boldsymbol{p}^{23} = \{q_2 = 15, q_4 = 0\}$, $\boldsymbol{p}^{24} = \{q_2 = 25, q_3 = 0\}$,
$\boldsymbol{p}^{25} = \{q_2 = 25, q_4 = 0\}$, $\boldsymbol{p}^{26} = \{q_1 = \pi, q_2 = 15\}$,
$\boldsymbol{p}^{27} = \{q_1 = \pi, q_2 = 25\}$, $\boldsymbol{p}^{28} = \{q_1 = \pi, q_3 = 0\}$.

Using the intersection of the singular surfaces and perturbation method, we obtain the final volume, which is the removed material, shown in Fig. 9.

Boundary patches of material removed are presented in Table 1. The volume of material removed is computed as 1487.6503.

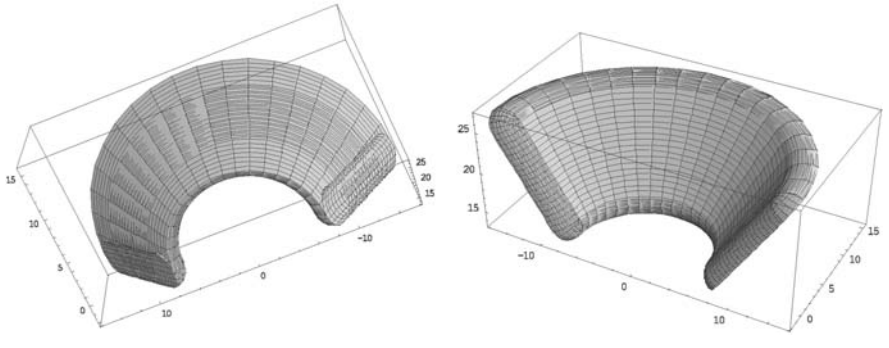

Fig. 9. Two views of the removed material

5 Five-parameter verification

Consider the NC verification of a process involving the motion of a cutting tool represented by a surface given by:

$$\boldsymbol{\Gamma}(u, v) = [5\cos v\, 5 + u\, 5 \sin v]^T , \tag{29}$$

with the following geometric constraints $5 < u < 10$, and $0 < v < \pi/2$. The machining operation will sweep the surface $\boldsymbol{\Gamma}$ along one axis with rotation matrix

$$\boldsymbol{R}_3(v_3) = \begin{bmatrix} \sin v_3 & 0 & \cos v_3 \\ -\cos v_3 & 0 & \sin v_3 \\ 0 & -1 & 0 \end{bmatrix} \text{ and } \boldsymbol{\Psi}_3 = [0\,0\,0]^T , \tag{30}$$

along another axis with rotation matrix

$$\boldsymbol{R}_2 = \begin{bmatrix} 1 & 0 & 0 \\ 0 & 0 & 1 \\ 0 & -1 & 0 \end{bmatrix} \text{ and } \boldsymbol{\Psi}_2(v_2) = [0\,0\,v_2 + 7]^T , \tag{31}$$

followed by a translation

$$\boldsymbol{R}_1 = \begin{bmatrix} 10 & 0 & \\ 0 & 0 & -1 \\ 0 & 1 & 0 \end{bmatrix} \text{ and } \boldsymbol{\Psi}_1(v_1) = [0\,0\,v_1 + 10]^T ,$$

subject to the following constraints$10 \le v_1 \le 20$, $7 \le v_2 \le 15$, and $-\pi/2 \le v_3 \le \pi/2$, shown in Fig. 10. As this is a five-parameter verification, the resulting Jacobian is (3×5). A total

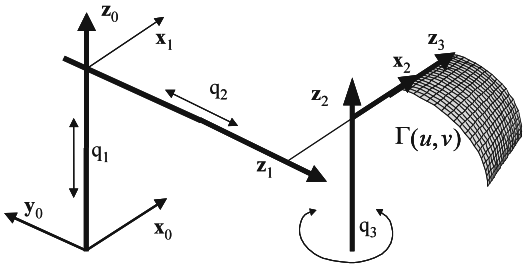

Fig. 10. A five-parameter verification

of 90 singular sets exist. For example, singularities due to the boundary singular behavior produced by the limits of v_1, v_3, u are shown in Fig. 11. The complete swept volume of the five-parameter sweep is shown in Fig. 12.

Because of the unique properties of the swept volume formulation, variation effects due to machining amount changes of different axes can be addressed. Consider, for example, introducing a change in the upper limits of the machining parameters: a change in the upper limit of v_3 from $\pi/2$ to $\pi/4$; a change in the upper limit of u from 10 to 8; and a change in the upper limit of v from $\pi/2$ to $\pi/4$. The verification can be readily updated as shown in Fig. 13.

A note on accuracy

The formulation for swept volumes is exact and does not depend on any approximation. The only approximation arises in comput-

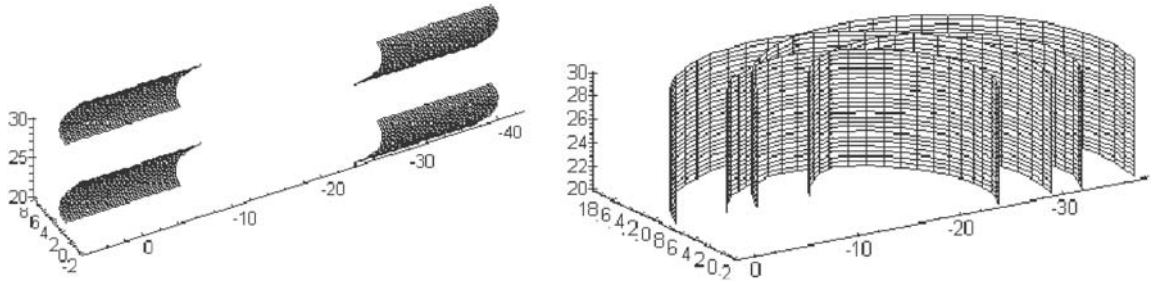

Fig. 11. Singular surfaces

Fig. 12. Material removed for 5-axis verification

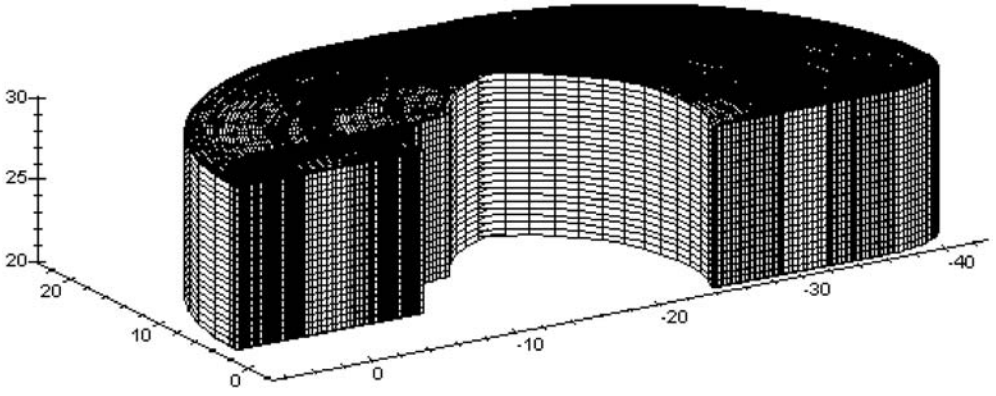

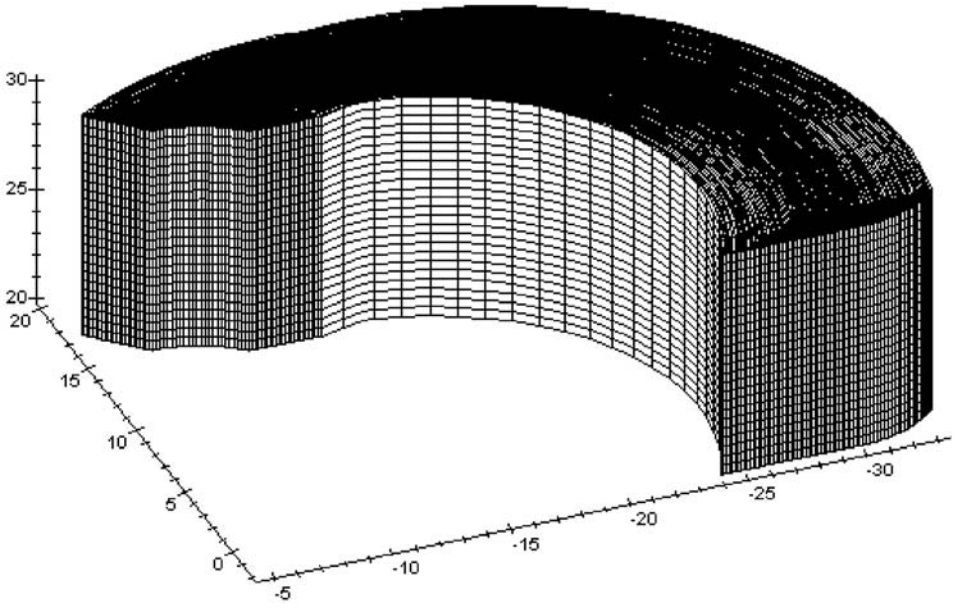

Fig. 13. The updated verification due to machining parameter variations

ing sections through the manifold, since a numerical method is implemented to obtain traces of each variety on a cutting plane. In addition, volume computation involves a numerical integration algorithm that is inherently tolerance-dependent.

6 Conclusions

A formulation for representing material removed in a machining verification process of up to n-parameters has been presented. The material removed was formulated in terms of generalized coordinates including inequality constraints imposed on the object's dimensions and sweep geometry. Inequality constraints were transformed to equality constraints and included in the analysis. It was observed that varieties produced from the swept volume are characterized by a rank-deficiency condition. It was also observed that the perturbation method can be used to determine the boundary surface: the swept volume. The strength of this formulation lies in its ability (1) to simulate the verification process, in terms of boundary surfaces, to the material removal as parametric equations, (2) to identify the boundary, and (3) to compute the volume of material removed.

References

1. Wang WP, Wang KK (1986) Geometric modeling for swept volume of moving solids. IEEE Comput Graph Appl 6(12):8
2. Boussac S, Crosnier A (1996) Swept volumes generated from deformable objects application to NC verification. Proceedings of the 13th IEEE International Conference on Robotics and Automation, Minneapolis, MN, 1996, vol 2, pp 1813–1818
3. Liu C, Esterling D (1997) Solid modeling of 4-axis wire EDM cut geometry. Comput Aided Des 29(12):803
4. Chiou JCJ (2004) Accurate tool position for five-axis rule surface machining by swept envelope approach. Comput Aided Des 36(10):967
5. Lartigue C, Duc E, Affouard A (2003) Tool path deformation in 5-axis flank milling using envelope surface. Comput Aided Des 35(4):375
6. Roth D, Bedi S, Ismail F, Mann S (2001) Surface swept by a toroidal cutter during 5-axis machining. Comput Aided Des 33(1):57
7. Blackmore D, Leu MC, Wang LP, Jiang H (1997) Swept volumes: a retrospective and prospective view. Neural Parallel Sci Comput 5:81
8. Leu MC, Wang L, Blackmore D (1997) Verification program for 5-axis NC machining with general APT tools. Ann CIRP 46(1):419
9. Voelker HB, Hunt WA (1985) The role of solid modeling in machining process modeling and NC verification. SAE Technical Paper 810195, Warrendale, PA
10. Menon JP, Voelcker HB (1992) Toward a comprehensive formulation of NC verification as a mathematical and computational problem. Proceedings of the 1992 Winter Annual Meeting of ASME, Anaheim, CA, 1992, vol 59, pp 147–164
11. Oliver J, Goodman E (1990) Direct dimensional NC verification. Comput Aided Des 22:3
12. Narvekar AP, Huang Y, Oliver J (1992) Intersection of rays with parametric envelope surfaces representing five-axis NC milling tool swept volumes. Proceedings of the 1992 18th Annual ASME Design Automation Conference, Scottsdale, AZ, 1992, vol 44, pp 223–230
13. Takata S, Tsai MD, Inui M (1992) A cutting simulation system for machinability evaluation using a workpiece model. Ann CIRP 38:539
14. Jerard R, Drysdale R (1988) Geometric simulation of numerical control machinery. ASME Comput Eng 2:129
15. Jerard R, Drysdale R (1991) Methods for geometric modeling, simulation, and spatial verification of NC machining programs. In: Wozny MJ, Turner JU, Pegna J (ed) Product modeling for computer-aided design. North Holland, Amsterdam, pp 1–14
16. Koren Y, Lin RS (1995) Five-axis surface interpolators. Ann CIRP 44(1):379
17. Menon JP, Robinson DM (1993) Advanced NC verification via massively parallel raycasting. ASME Manufact Rev 6:141
18. Oliver JH (1990) Efficient intersection of surface normals with milling tool swept volumes for discrete three-axis NC verification. ASME Des Autom Conf 23(1):159
19. Liang X, Xiao T, Han X, Ruan JX (1997) Simulation software GNCV of NC verification author affiliation. ICIPS Proceedings of the 1997 IEEE International Conference on Intelligent Processing Systems, Beijing, China, 1997, vol 2, pp 1852–1856
20. Liu C, Esterling DM, Fontdecaba J, Mosel E (1996) Dimensional verification of NC machining profiles using extended quadtrees. Comput Aided Des 28(11):845

21. Lee YS (1998) Non-isoparametric tool path planning by machining strip evaluation for 5-axis sculptured surface machining. Comput Aided Des 30(7):559
22. Lo CC (1999) Efficient cutter-path planning for five-axis surface machining with a flat-end cutter. Comput Aided Des 31(9):557
23. Chiou CJ, Lee YS (1999) A shape-generating approach for multi-axis machining *G*-buffer models. Comput Aided Des 31(12):761
24. Chiou CJ, Lee YS (2002) A machining potential field approach to tool path generation for multi-axis sculptured surface machining. Comput Aided Des 34(5):357
25. Elber G, Cohen E (1999) A unified approach to verification in 5-axis freeform milling environments. Comput Aided Des 31(13):795
26. Balasubramaniam M, Laxmiprasad P, Sarma S, Shaikh Z (2000) Generating 5-axis NC roughing paths directly from a tessellated representation. Comput Aided Des 32(4):261
27. Balasubramaniam M, Ho S, Sarma S, Adachi Y (2002) Generation of collision-free 5-axis tool paths using a haptic surface. Comput Aided Des 34(4):267
28. Rao A, Sarma R (2000) On local gouging in five-axis sculptured surface machining using flat-end tools. Comput Aided Des 32(7):409
29. Jensen CG, Red WE, Pi J (2002) Tool selection for five-axis curvature matched machining. Comput Aided Des 34(3):251
30. Bohez ELJ (2002) Compensating for systematic errors in 5-axis NC machining. Comput Aided Des 34(5):391
31. Mann S, Bedi S (2002) Generalization of the imprint method to general surfaces of revolution for NC machining. Comput Aided Des 34(5):373
32. Yoon JH, Pottmann H, Lee YS (2003) Locally optimal cutting positions for 5-axis sculptured surface machining. Comput Aided Des 35(1):69
33. Bedi S, Mann S, Menzel C (2003) Flank milling with flat end milling cutters. Comput Aided Des 35(3):293
34. Gray P, Bedi S, Ismail F (2003) Rolling ball method for 5-axis surface machining. Comput Aided Des 35(4):347
35. Gray P, Ismail F, Bedi S (2004) Graphics-assisted rolling ball method for 5-axis surface machining. Comput Aided Des 36(7):653
36. Fussell BK, Jerard RB, Hemmett JG (2003) Modeling of cutting geometry and forces for 5-axis sculptured surface machining. Comput Aided Des 35(4):333
37. Lauwers B, Dejonghe P, Kruth JP (2003) Optimal and collision free tool posture in five-axis machining through the tight integration of tool path generation and machine simulation. Comput Aided Des 35(5):421
38. Jun CS, Cha K, Lee YS (2003) Optimizing tool orientations for 5-axis machining by configuration-space search method. Comput Aided Des 35(6):549
39. Bohez ELJ, Minh NTH, Kiatsrithanakorn B, Natasukon P, Huang RY, Son LT (2003) The stencil buffer sweep plane algorithm for 5-axis CNC tool path verification. Comput Aided Des 35(12):1129
40. Langeron JM, Duc E, Lartigue C, Bourder P (2004) A new format for 5-axis tool path computation, using B-spline curves. Comput Aided Des 36(12):1219–1229
41. Abdel-Malek K, Yeh H (1997) Geometric representation of the swept volume using Jacobian rank-deficiency conditions. Comput Aided Des 29(6):457
42. Abdel-Malek K, Yeh HJ, Othman S (1998) Swept volumes, void and boundary identification. Comput Aided Des 30(13):1009
43. Abdel-Malek K, Yeh HJ (1997) Analytical boundary of the workspace for general 3-DOF mechanisms. Int J Robot Res 16(2):1
44. Blackmore D, Leu MC, Wang LP (1997) Sweep-envelope differential equation algorithm and its application to NC machining verification. Comput Aided Des 29(9):629
45. Ahn JC, Kim MS, Lim SB (1997) Approximate general sweep boundary of 2D curved object. Comput Vis Graph Image Process 55:98
46. Elber G (1997) Global error bounds and amelioration of sweep surfaces. Comput Aided Des 29:441
47. Ling ZK, Chase T (1996) Generating the swept area of a body undergoing planar motion. ASME J Mech Des 118:221
48. Sourin A, Pasko A (1996) A function representation for sweeping by a moving solid. IEEE Trans Vis Comput Graph 2:11
49. Abdel-Malek K, Yeh HJ (1996) Determining intersection curves between surfaces of two solids. Comput Aided Des 28(6/7):539